

Analysis of Transport Phenomena in Concrete Walls Exposed to Hot Gas

Jatuporn Stakulcharoen, Watit Pakdee, and Phadungsak Ratanadecho*

Research Center of Microwave Utilization in Engineering (RCME)
Department of Mechanical Engineering, Faculty of Engineering, Thammasat University,
Rangsit Campus, 99 Mu 18, Klong Luang, Pathumthani 12120 ,Thailand
Tel: 0-2564-3001-9, *E-mail: ratphadu@engr.tu.ac.th

*(Corresponding Author)

Abstract

The phenomena of coupled heat and mass transfer in concrete structures exposed to hot gas is investigated to help improving fire safety assessment. This study develops a mathematical model, simulating the coupled heat and mass transfer in concrete structures that are exposed to hot gas. The different conditions with and without gravitational force are considered. Three different values of saturation were initialized. The concrete structure is assumed as an unsaturated porous medium. The finite volume method – the principle of Newton-Raphson method – was implemented. Effects of prescribed boundary conditions and initial saturations on associated variables, *e.g.*, gas pressure, temperature, moisture content, were investigated. The transient heating boundary profoundly affects the mechanisms of heat and mass transfer.

Keywords: coupled heat and mass transfer, unsaturated porous medium, finite volume method, concrete walls.

1. Introduction

The knowledge of concrete behaviors under hot gas – changes in the internal total pressure, temperature and saturation in the structure with time as well as their distributions – is important in the safety assessment of buildings. The problem of heat and mass transfer in concrete exposed to hot gas, involving pressure, temperature and moisture content distributions, multiphase mass transfer (as liquid and gaseous phases), and highly non-linear dependence of various material parameters of concrete, includes complex processes.

The analysis of heat and mass transfer in porous materials has been the subject of theoretical and experimental work[1,2]. Most theories have been proposed to explain the physical phenomena of drying process in porous materials: the diffusion theory the capillary flow theory and the evaporation-condensation theory. A convenient starting point of drying theory is careful, in the work of Whitaker[3] and Patankar [4]who has derived appropriate locally volume averaged conservation equations for two-phase capillary flow in porous media. The mathematical models for

simultaneous heat and mass transfer during convective drying of porous media have been studied extensively (Boukadida and Ben Nasrallah[5], Perre and Turner[6]). Almost all the previous models that are based on Whitaker's theory, takes into account the thermal and mass transfer as well as total gaseous pressure. Recently, Ratanadecho et al. [7-9] carried out the systematical study on drying process of multi-layered porous packbed using microwave energy. The recent developments in high temperature convective drying are presented by P.Perre et al [10]. The process has been investigated experimentally and theoretically for two drying fluids : moist air and superheated steam, and for two materials which are light concrete and softwood. S. Ben Nasrallah and P.Perre [11] studied the model of heat and mass transfer in porous media deduced from Whitaker's theory. It leads to a very comprehensive set of equations and takes into account the effect of the gaseous pressure. The problem is numerically solved with unidirectional transfers. The evolution of temperature moisture content and pressure as well as the overall drying kinetics are calculated for two very different porous media.

C. L. D. Huang et al [12] developed a mathematical model, simulating the coupled heat and mass transfer in concrete structures at elevated temperatures as fire. The numerical results predicted the phenomenon of "moisture clog" and the explosive spalling of concrete under fire. The investigations showed that the seal layer as a fire protection had significant effects on the pore pressure buildup in the concrete walls, which, in turn, improved the susceptibility of fire damage. The assumptions concerning the porous system and the transport process were multi-phase, solid rigid and incompressible liquid. Mobility of liquid was assumed to be negligible. In addition, compressional work, energy transferred by diffusion and viscous dissipation were neglected.

This study develops a mathematical model, simulating heat and mass transfer in concrete structure undergone different conditions. The concrete is considered as the unsaturated porous medium. This model provides careful consideration of changes in internal total pressure, temperature and moisture during hot gas exposure period.

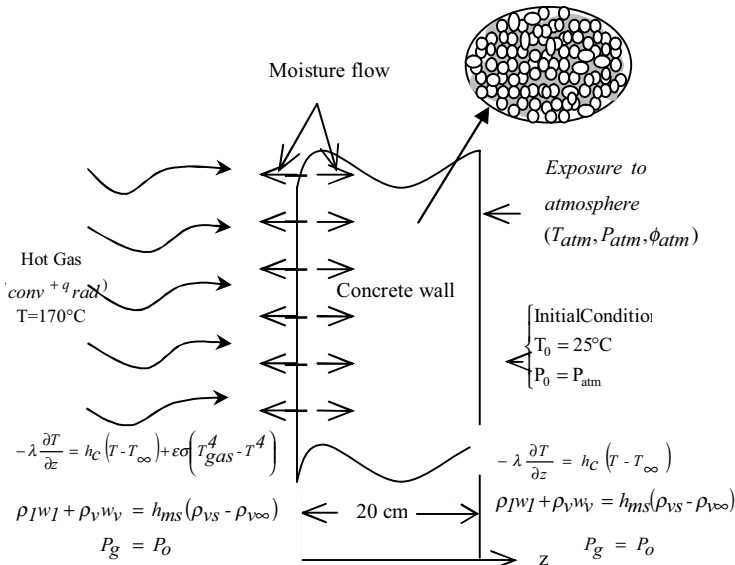


Figure1. Physical model of concrete wall exposed to hot gas

2. Governing equations

A one-dimensional concrete slab exposed to hot gas is shown schematically in figure 1. One surface of the slab ($z=0$) is exposed to hot gas at 170 °C. The other surface of the concrete slabs ($z=20$ cm) remains under atmospheric conditions, allowing the heat and mass to transfer freely through the surface to the ambient. This schematic can be applied to the other dimensional concretes exposed to hot gas in case without gravitational force.

Concrete is a non-hygroscopic porous medium which has the advantages of being homogeneous, isotropic and reproducible. It has low porosity of 0.16 and also a high permeability of 8.41×10^{-12} . Local thermodynamic equilibrium among each phase is assumed. With conservation of mass and energy in concrete wall, the main basic governing equation of mass and energy for all phase can be derived using finite control volume method. The microscopic mass conservation equations for liquid, water vapor, air and gas phase, are used. [1]

Moisture Equation:

The phenomenon of moisture transport is described by the mass conservation equations for the liquid phase and the water vapor portion of the gas phase since it is the total water content that is of interest, these equations in one-dimensional forms can be added together to yield an equation for the total moisture content as follows:

$$\phi \frac{\partial}{\partial t} \{ \rho_l s + \rho_v (1-s) \} + \frac{\partial}{\partial z} [\rho_l w_l + \rho_v w_v] = 0 \quad (1)$$

Pressure Equation:

The internal total pressure is derived from air phase as

$$\frac{\partial}{\partial t} \{ \rho_a \phi (1-s) \} + \frac{\partial}{\partial z} [\rho_a w_a] = 0 \quad (2)$$

Energy equation:

The temperature of the concrete wall exposed the hot air stream with fixed characteristics is obtained by solving the conventional heat transport equation considering the enthalpy transport based on the water and gas flows, the conduction heat and latent heat transfer due to evaporation, the energy conservation equation is represented by:

$$\frac{\partial}{\partial t} [(\rho c_p)_T T] + \nabla [\{ \rho_l c_{pl} w_l + (\rho_a c_{pa} + \rho_v c_{pv}) w_g \} T] = - \nabla q + h_v n \quad (3)$$

State Equations:

The gas phase is assumed to be an ideal mixture of vapor phase and air phase, so that the species density can be determined by the state equations, with the classical definitions for total density of the gas, ρ_g , and the mass average velocity of the gas. [4]

Phenomenological and Equilibrium Relations

In order to complete the system of equations, the expressions for the superficial average velocity of the liquid and gas phases the generalized Darcy's law in the following form is used. [3] For the velocity of vapor water and air phase the generalized Fick's law for a two-component gas mixture can be determined. [4] By using the following definitions:

$$\frac{\rho_a}{\rho_l} = Y_a$$

$$\frac{\rho_v}{\rho_l} = Y_v, \quad \frac{\rho_g}{\rho_l} = Y_g, \quad \frac{Y_v}{Y_g} = W_v, \quad (4)$$

we obtained the moisture equation, written as

$$\phi \frac{\partial}{\partial t} \{ s + Y_v (1-s) \} + \frac{\partial}{\partial z} \left[\frac{KK_{rl}}{\mu_l} \left(\frac{\partial p_c}{\partial z} - \frac{\partial p_g}{\partial z} + g_z \right) + Y_v \frac{KK_{rg}}{\mu_g} \left(- \frac{\partial p_g}{\partial z} + \rho_g g_z \right) - Y_g D_m \frac{\partial}{\partial z} (W_v) \right] = 0 \quad (5)$$

After manipulation with Darcy's law and Fick's law, the internal total pressure equation is given by

$$\phi \frac{\partial}{\partial t} \{ Y_a (1-s) \} + \frac{\partial}{\partial z} \left[Y_a \frac{KK_{rg}}{\mu_g} \left(- \frac{\partial p_g}{\partial z} + \rho_g g_z \right) - Y_g D_m \frac{\partial}{\partial z} \left(\frac{\rho_a}{\rho_g} \right) \right] = 0 \quad (6)$$

Also, the energy equation in terms of temperature can be expressed as

$$\frac{\partial}{\partial t} \left\{ (\rho c_p)_T T \right\} + \frac{\partial}{\partial z} \left[\left\{ \rho_l c_{pl} w_l + (\rho_a c_{pa} + \rho_v c_{pv}) w_g \right\} T \right] = \frac{\partial}{\partial z} \left[\lambda \frac{\partial T}{\partial z} \right] - h_{iv} \left\{ \frac{\partial}{\partial t} \left[\rho_v \phi (1-s) \right] + \frac{\partial}{\partial z} \left[\rho_v \frac{KK_{rg}}{\mu_g} \left(-\frac{\partial P_g}{\partial z} + \rho_g g_z \right) - \rho_g D_m \frac{\partial}{\partial z} \left(\frac{\rho_v}{\rho_g} \right) \right] \right\} \quad (7)$$

The symbol S denotes water saturation that is related to the effective water saturation S_e as shown by the equation below

$$S_e = \frac{S - S_{ir}}{1 - S_{ir}} \quad (8)$$

where S_{ir} is the irreducible water saturation.

Boundary Conditions and initial conditions

The boundary conditions proposed for the permeable heating surface, for the exchange of energy at the open boundary with convection and radiation ,can be described as in the following:

$$-\lambda \frac{\partial T}{\partial z} = h_c (T - T_\infty) + \epsilon \sigma (T_{gas}^4 - T^4) \quad (9)$$

Mass transfer at the permeable surface is modeled by means of a locally constant mass transfer coefficient, which is related to the local water vapor flux density:

$$\rho_l w_l + \rho_v w_v = h_{ms} (\rho_{vs} - \rho_{v\infty}) \quad (10)$$

The mass transfer coefficient, h_{ms} , at the permeable surface or upper surface depends on the surface saturation coefficient which varies with varying average water saturation. The total pressure at permeable surface can be defined as:

$$P_g = P_0, \quad (11)$$

where P_0 is atmospheric pressure

Furthermore, in the case without gravitational force, the above equations can still be applied, in which the terms involving the gravitational force are neglected.

3. Numerical Method

The coupled non-linear set of heat and mass equations with regard to water saturation or pressure of gas phase, P_g and temperature, T_s , were solved numerically by using the finite control volume. The advantage of this method is that it ensures flux conservation, and thus avoiding generation of parasitic sources. The basic strategy of finite control volume discretization method is to divide the calculated domain into a number of control volumes [14] and then integrate

the conservation equations over this control volume over an interval of time. At the boundaries of the calculated domain, the conservation equations were discretized by integrating over half the control volume and by taking into account the boundary conditions. At the corners of the calculated domain we used a quarter of control volume. At each time increment, the nodal value of moisture content, internal total pressure and temperature were solved iteratively. The Newton-Raphson method was employed at each iteration to improve the convergence rate.

The volume average technique is applied to the moisture transport (Eq.(1)). The discretized form of Eq.(1) is given by

$$\frac{\phi}{\Delta t} (1 - s_{ir}) \left\{ (s_{ek}^{n+1} - s_{ek}^n) + (Y_{vk}^{n+1} (1 - s_{ek}^{n+1}) - Y_{vk}^n (1 - s_{ek}^n)) \right\} + \frac{1}{\Delta z} \left\{ \begin{aligned} & \left[\frac{KK_{rl}}{\mu_l} \Big|_{k+\frac{1}{2}} \left(\left(\frac{P_{ck+1}^{n+1} - P_{ck}^{n+1}}{\Delta z} \right) - \left(\frac{P_{gk+1}^{n+1} - P_{gk}^{n+1}}{\Delta z} \right) + g_z \right) \right. \\ & \left. - \frac{KK_{rl}}{\mu_l} \Big|_{k-\frac{1}{2}} \left(\left(\frac{P_{ck}^{n+1} - P_{ck-1}^{n+1}}{\Delta z} \right) - \left(\frac{P_{gk}^{n+1} - P_{gk-1}^{n+1}}{\Delta z} \right) + g_z \right) \right] \\ & + Y_{vk}^{n+1} \left[\frac{KK_{rg}}{\mu_g} \Big|_{k+\frac{1}{2}} \left(-\left(\frac{P_{gk+1}^{n+1} - P_{gk}^{n+1}}{\Delta z} \right) + \rho_g g_z \right) \right. \\ & \left. - \rho_{vk-1}^{n+1} \frac{KK_{rg}}{\mu_g} \Big|_{k-\frac{1}{2}} \left(-\left(\frac{P_{gk}^{n+1} - P_{gk-1}^{n+1}}{\Delta z} \right) + \rho_g g_z \right) \right] \\ & - Y_{gk}^{n+1} \left[D_{mk+\frac{1}{2}}^{n+1} \left(\frac{W_{vk+1}^{n+1} - W_{vk}^{n+1}}{\Delta z} \right) \right. \\ & \left. - D_{mk-\frac{1}{2}}^{n+1} \left(\frac{W_{vk}^{n+1} - W_{vk-1}^{n+1}}{\Delta z} \right) \right] \end{aligned} \right\} = 0 \quad (12)$$

Similarly, the discretized form of pressure equation (Eq.(2)) can be written as

$$\frac{\phi}{\Delta t} \left\{ (1 - s_{ir}) \left[Y_{ak}^{n+1} (1 - s_{ek}^{n+1}) - Y_{ak}^n (1 - s_{ek}^n) \right] \right\}$$

$$+ \frac{1}{\Delta z} \left\{ \begin{array}{l} Y_{ak}^{n+1} \left[\begin{array}{l} \frac{KK_{rg}}{\mu_g} \Big|_{k+\frac{1}{2}} \left(- \left(\frac{P_{gk+1}^{n+1} - P_{gk}^{n+1}}{\Delta z} \right) + \rho_g g_z \right) \\ - \frac{KK_{rg}}{\mu_g} \Big|_{k-\frac{1}{2}} \left(- \left(\frac{P_{gk}^{n+1} - P_{gk-1}^{n+1}}{\Delta z} \right) + \rho_g g_z \right) \end{array} \right] \\ D_{mk}^{n+1} \frac{1}{\Delta z} \left(\frac{\rho_a}{\rho_g} \Big|_{k+1}^{n+1} - \frac{\rho_a}{\rho_g} \Big|_k^{n+1} \right) \\ - Y_{gk}^{n+1} \left[\begin{array}{l} D_{mk}^{n+1} \frac{1}{\Delta z} \left(\frac{\rho_a}{\rho_g} \Big|_{k+1}^{n+1} - \frac{\rho_a}{\rho_g} \Big|_k^{n+1} \right) \\ - D_{mk}^{n+1} \frac{1}{\Delta z} \left(\frac{\rho_a}{\rho_g} \Big|_k^{n+1} - \frac{\rho_a}{\rho_g} \Big|_{k-1}^{n+1} \right) \end{array} \right] \end{array} \right\}$$

$$= 0 \tag{13}$$

Also, the discretized form of heat transport equation (Eq.(3)) can be written as

$$\frac{(\rho c_p)_{Tk}^{n+1} T_k^{n+1} - (\rho c_p)_{Tk}^n T_k^n}{\Delta t} + \frac{\rho l c_{pl}}{\Delta z} (w_{tk}^{n+1} T_k^{n+1} - w_{tk-1}^{n+1} T_{k-1}^{n+1})$$

$$+ \frac{(\rho c_p)_{av}}{\Delta z} (w_{gk}^{n+1} T_k^{n+1} - w_{gk-1}^{n+1} T_{k-1}^{n+1})$$

$$- \frac{1}{\Delta z} \left[\lambda_{k+\frac{1}{2}}^{n+1} \left(\frac{T_{k+1}^{n+1} - T_k^{n+1}}{\Delta z} \right) - \lambda_{k-\frac{1}{2}}^{n+1} \left(\frac{T_k^{n+1} - T_{k-1}^{n+1}}{\Delta z} \right) \right]$$

$$+ \frac{h_{lv} \rho_v \phi}{\Delta t} \left\{ (1 - s_{ir}) (s_{ek}^{n+1} - s_{ek}^n) \right\}$$

$$- \frac{1}{\Delta z} \left\{ \begin{array}{l} \rho_{vk}^{n+1} \frac{KK_{rg}}{\mu_g} \Big|_{k+\frac{1}{2}} \left(- \left(\frac{P_{gk+1}^{n+1} - P_{gk}^{n+1}}{\Delta z} \right) + \rho_g g_z \right) \\ - \rho_{vk-1}^{n+1} \frac{KK_{rg}}{\mu_g} \Big|_{k-\frac{1}{2}} \left(- \left(\frac{P_{gk}^{n+1} - P_{gk-1}^{n+1}}{\Delta z} \right) + \rho_g g_z \right) \end{array} \right\}$$

$$- \frac{1}{\Delta z} \left\{ \begin{array}{l} \rho_{gk}^{n+1} D_{mk}^{n+1} \frac{1}{\Delta z} \left(\frac{\rho_v}{\rho_g} \Big|_{k+1}^{n+1} - \frac{\rho_v}{\rho_g} \Big|_k^{n+1} \right) \\ - \rho_{gk-1}^{n+1} D_{mk-1}^{n+1} \frac{1}{\Delta z} \left(\frac{\rho_v}{\rho_g} \Big|_k^{n+1} - \frac{\rho_v}{\rho_g} \Big|_{k-1}^{n+1} \right) \end{array} \right\}$$

$$= 0 \tag{14}$$

The coupled non-linear set of Eq.(12)-Eq.(14) in regard to water saturation or moisture content, pressure, and temperature were solved numerically by using the finite control volume method. [13] The detail of the computational schemes and strategy are illustrated in figure 2.

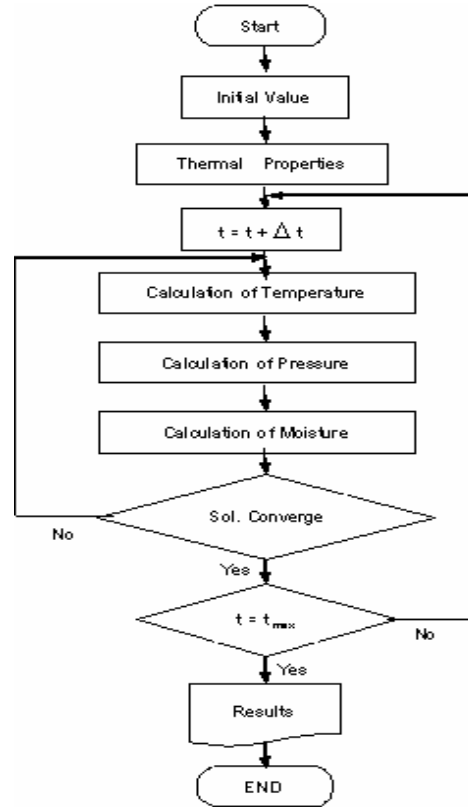


Figure 2. Computational scheme.

4. Results and Discussions

In one-dimensional porous concrete slabs exposed to hot gas, one surface of the slab (z=0) is exposed to hot gas at 170 °C. The other surface of the concrete slabs (z=20 cm) remains under atmospheric conditions, allowing the heat and mass to freely transfer from the medium surface to the surrounding.

The case without gravitational force is first implemented. The effect of initial saturation, S_{in}, of concrete is investigated based on three different values of saturation. The saturations of 0.1, 0.3, 0.7 are initialized within the domain. The first case of S_{in} = 0.1 is examined. The resulting plots of temperature distribution at various times are shown in figure 3. It is obvious that, at each time, temperature is highest at the heated surface due to the existence of the hot gas. At the locations away from the hot surface, the temperature decreases and becomes equal to the ambient temperature at the cold boundary. The steep curve of temperature near the hot surface indicates a high rate of heat transfer. Additionally, the overall temperature increases with time. It is observed from pressure distribution shown in figure 4 that there appears the vacuum pressure on the early

time because the extraction of liquid increases the volume of the gaseous phase whereas air fills the voids slowly. At later times from 2 hours, pressure builds up rapidly near the heated surface. Due to low initial saturation, liquid can easily moves through and fulfills the pores within the medium. In addition to this behavior, high diffusive vapor flux causes the gas pressure to increase. The pressure keeps going up with time. However, it remains vacuum in the colder regions in the beginning period. Saturation distribution is illustrated in figure 5. It is found that the saturation reduced fast, especially at the hot surface because of the high liquid extraction rate. After the early time, near the hot surface, the values of saturation reaches 0.06 which is the minimum saturation of concrete materials this condition refers to the dry zone condition. At this condition saturation is minimum. The amount of liquid inside the medium will not decrease after this stage. As a result, liquid is accumulated thereby causing the pressure buildup that can be observed in figure 4. Moreover, it is noticed that the peaks of pressure are located near the boundary of dry zone inside the concrete. This peak corresponds to the pressure that builds up since a liquid accumulates as it cannot be extracted further under the dry zone condition.

To gain more insights in effects of saturation, the results for the case of $S_{in} = 0.3$ and 0.7 are discussed. The distributions of temperature, pressure, and saturation are depicted for the case of $S_{in} = 0.3$, in figure 6- 8. Figures 9-11 represent the results of temperature, pressure, and saturation respectively for the case when S_{in} is 0.7 . The distribution profiles of all variables are similar between the two cases ($S_{in} = 0.3$ and $S_{in} = 0.7$). However, magnitudes of pressure is greater in the case of $S_{in} = 0.7$. The reason is that there is more amount of saturated water filled in pores. In case of $S_{in} = 0.3$, greater vacuum is observed due to larger rate of liquid extraction in which the volume of gas is enlarged. The result is more pronounced when $S_{in} = 0.7$. In terms of temperature variations, for small value of the initial saturation, temperature rises at a faster rate during the early simulation. This result is due to the presence of dry zone in the early times.

In what follow, the computed results under the condition that gravitational effect is considered are presented. The temperature distributions shown in figure 12, 15, and 18 are found similar to the case without gravitational force for various S_{in} of 0.1 , 0.3 , 0.7 respectively given in figure 3, 6 and 9. The saturation is low at distance near the top heated surface, while the values become high near the bottom surface. This phenomenon is caused by the gravitational effect that enhances the downward movement of liquid towards the bottom boundary. This observed result corresponds well with initial pressure variations that reveal the continuous increase of the pressure from the case with gravitational force to the bottom wall. It is clear that, also, the gravitational force influences the liquid transport behavior.

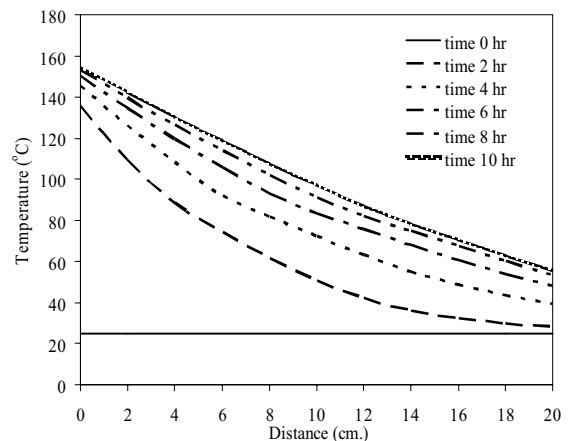


Figure 3. Temperature distribution as a function of depth and time from the structure exposed to hot gas from the case without gravitational force. ($S_{in} = 0.1$)

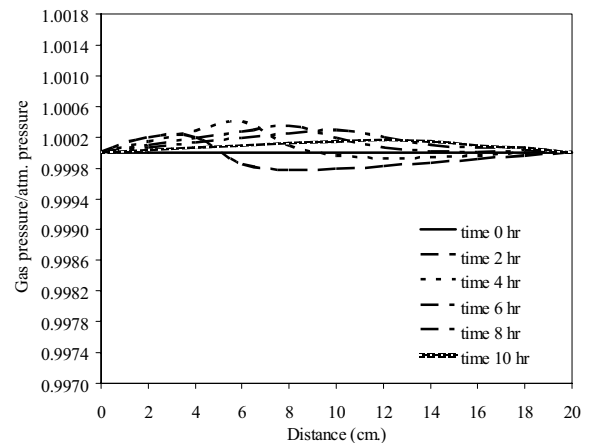


Figure 4. Pressure distribution as a function of depth and time from the structure exposed to hot gas from the case without gravitational force. ($S_{in} = 0.1$)

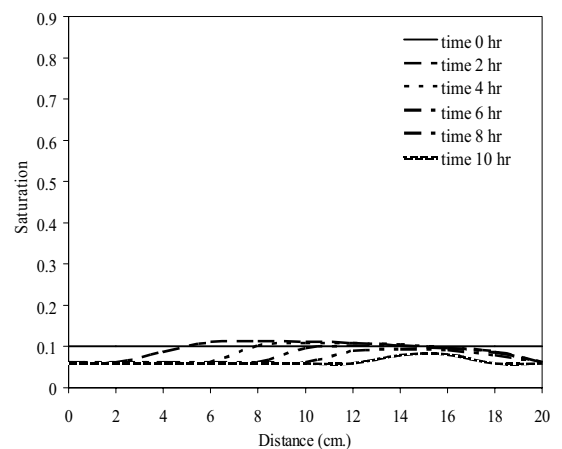


Figure 5. Saturation distribution as a function of depth and time from the structure exposed to hot gas from the case without gravitational force. ($S_{in} = 0.1$)

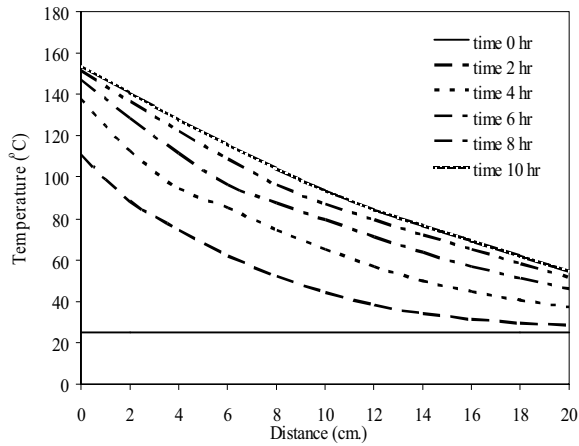


Figure 6. Temperature distribution as a function of depth and time from the structure exposed to hot gas from the case without gravitational force. ($S_{in} = 0.3$)

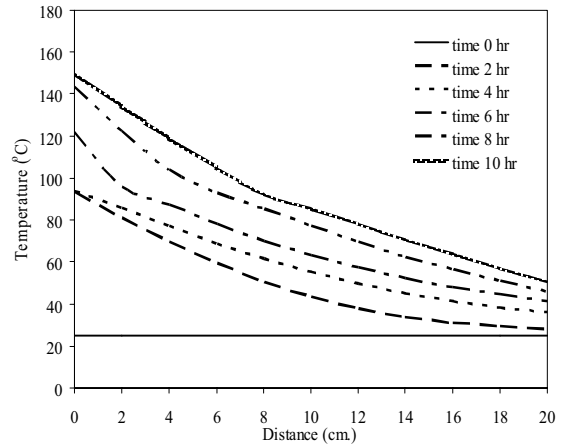


Figure 9. Temperature distribution as a function of depth and time from the structure exposed to hot gas from the case without gravitational force. ($S_{in} = 0.7$)

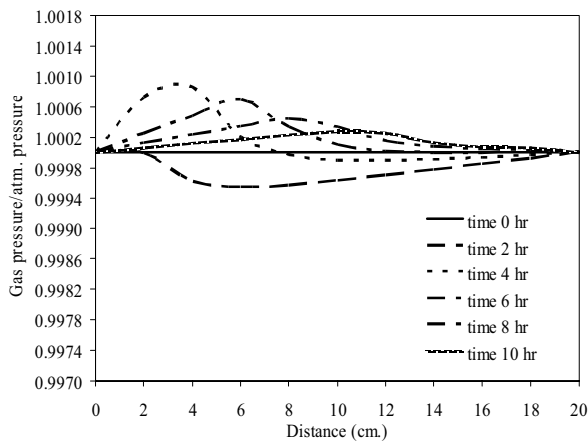


Figure 7. Pressure distribution as a function of depth and time from the structure exposed to hot gas from the case without gravitational force. ($S_{in} = 0.3$)

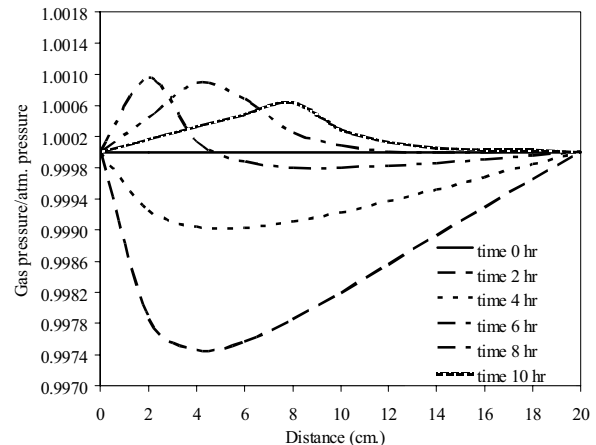


Figure 10. Pressure distribution as a function of depth and time from the structure exposed to hot gas from the case without gravitational force. ($S_{in} = 0.7$)

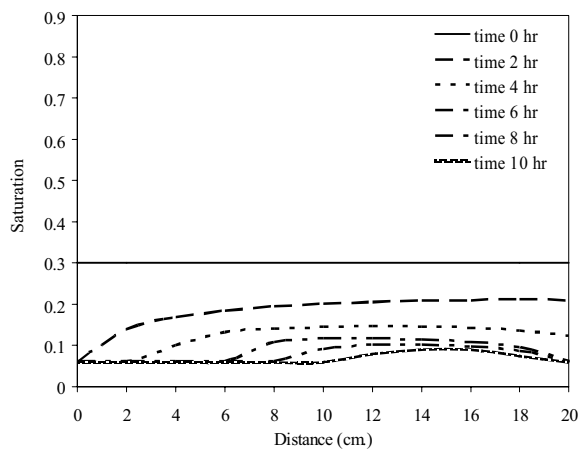


Figure 8. Saturation distribution as a function of depth and time from the structure exposed to hot gas from the case without gravitational force. ($S_{in} = 0.3$)

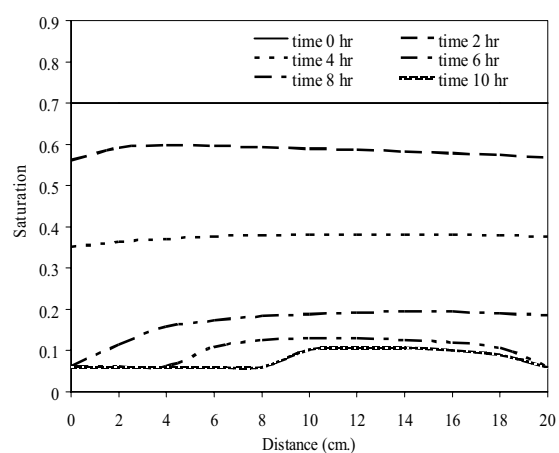


Figure 11. Saturation distribution as a function of depth and time from the structure exposed to hot gas from the case without gravitational force. ($S_{in} = 0.7$)

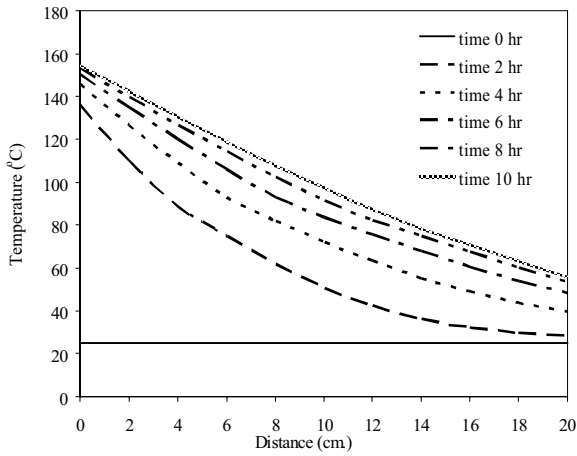


Figure 12. Temperature distribution as a function of depth and time from the structure exposed to hot gas from the case with gravitational force. ($S_{in} = 0.1$)

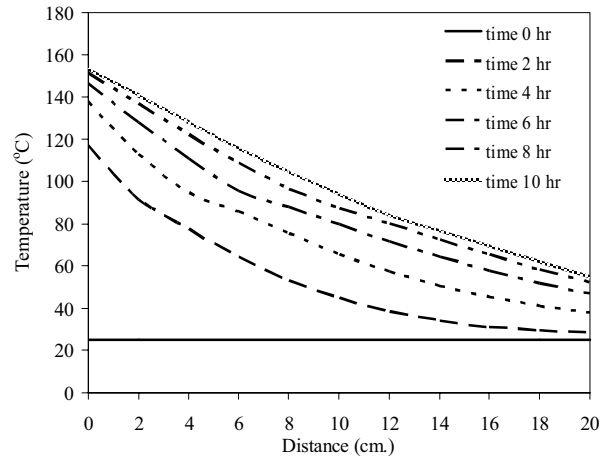


Figure 15. Temperature distribution as a function of depth and time from the structure exposed to hot gas from the case with gravitational force. ($S_{in} = 0.3$)

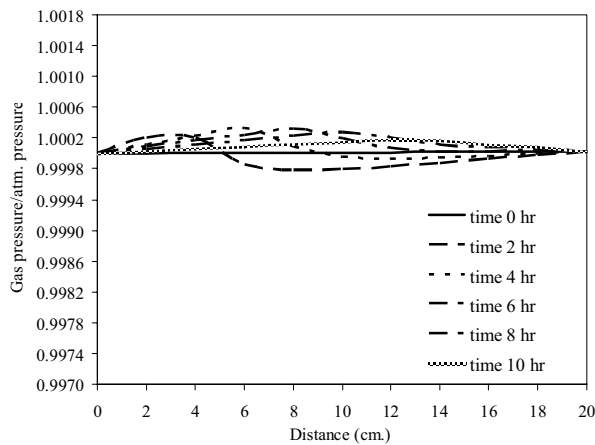


Figure 13. Pressure distribution as a function of depth and time from the structure exposed to hot gas from the case with gravitational force. ($S_{in} = 0.1$)

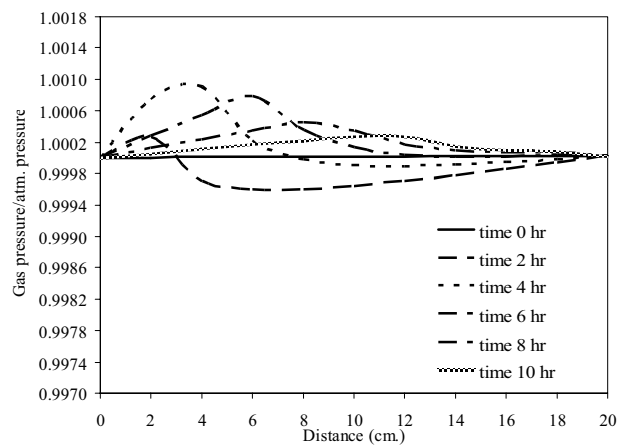


Figure 16. Pressure distribution as a function of depth and time from the structure exposed to hot gas from the case with gravitational force. ($S_{in} = 0.3$)

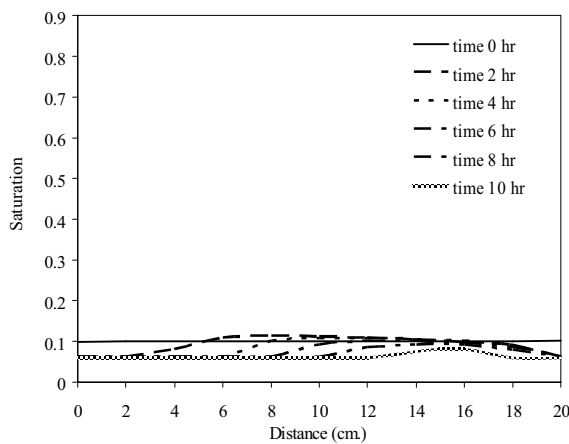


Figure 14. Saturation distribution as a function of depth and time from the structure exposed to hot gas from the case with gravitational force. ($S_{in} = 0.1$)

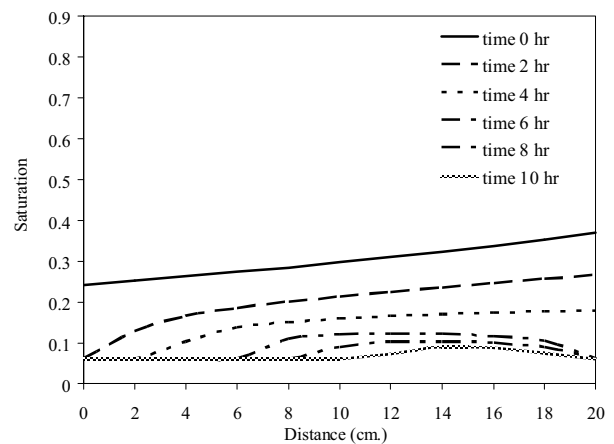


Figure 17. Saturation distribution as a function of depth and time from the structure exposed to hot gas from the case with gravitational force. ($S_{in} = 0.3$)

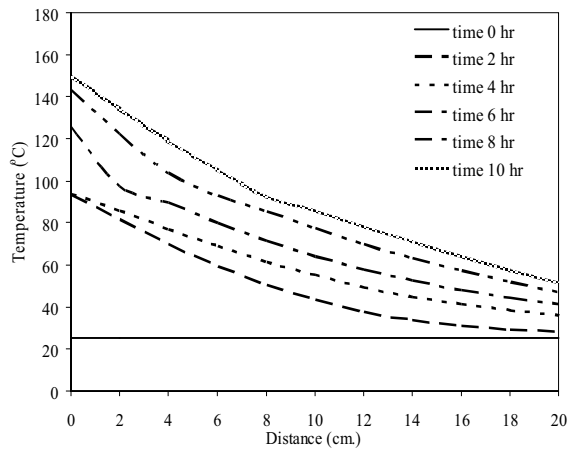


Figure 18. Temperature distribution as a function of depth and time from the structure exposed to hot gas from the case with gravitational force. ($S_{in} = 0.7$)

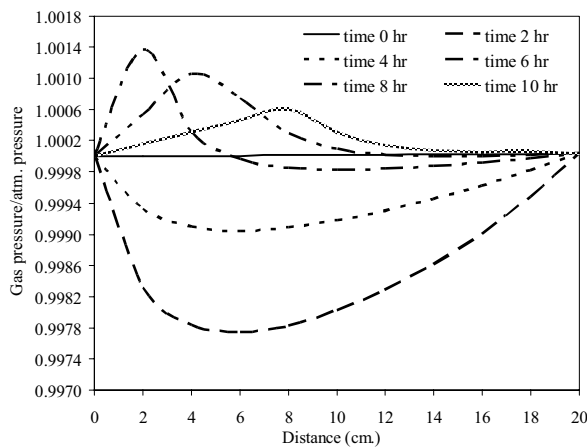


Figure 19. Pressure distribution as a function of depth and time from the structure exposed to hot gas from the case with gravitational force. ($S_{in} = 0.7$)

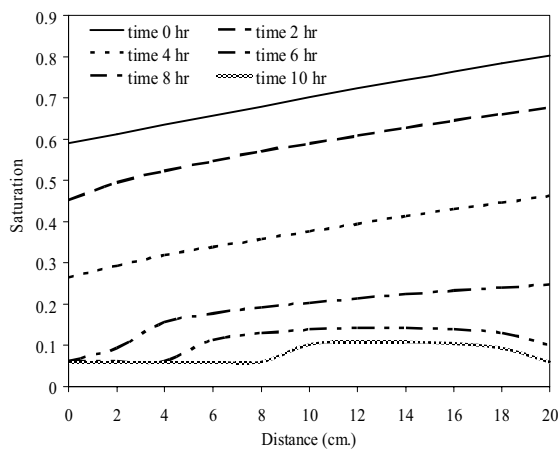


Figure 20. Saturation distribution as a function of depth and time from the structure exposed to hot gas from the case with gravitational force. ($S_{in} = 0.7$)

5. Conclusions

This study develops a mathematical model, simulating the coupled heat and mass transfer in concrete structures that are exposed to hot gas. The different conditions with and without gravitational force are considered. Three different initial saturations were applied. The finite volume method – the principle of Newton-Raphson method – was implemented. For all initial saturations, temperature is highest at the heated surface as a result of the existence of the hot gas. Due to low initial saturation, liquid can easily move through and fulfills the pores within the medium reducing the gas volume, which leads to pressure buildups near the hot wall. The peaks of pressure appear near the location where the dry zone ends. In overall, the concrete temperature as well as internal total pressure increases with time. In the case with gravitational effect, the value of saturation is higher at locations farther away from the heated surface. This phenomenon results from the gravitational effect that enhances the downward movement of liquid towards the bottom boundary.

Finally, the numerical simulation will be validated with published work. Our future work will focus on the effects of fire to concrete walls for the purpose of the fire safety assessment.

Notation

| | |
|-----------|--|
| D_m | = effective molecular mass diffusion (m^2/s) |
| S | = water saturation |
| T | = temperature ($^{\circ}C$) |
| H_v | = specific heat of vaporization (J/kg) |
| t | = time (s) |
| p | = pressure (Pa) |
| n | = phase change term ($kg/m^3 s$) |
| w | = velocity (m/s) |
| λ | = effective thermal conductivity ($W/m K$) |
| k | = permeability (m^2) |
| ϕ | = porosity |
| s | = saturation |
| g | = gravitational constant (m/s^2) |
| ρ | = density (kg/m^3) |
| μ_l | = dynamic viscosity of liquid (Pa s) |
| μ_g | = dynamic viscosity of gas (Pa s) |
| h_c | = heat transfer constant ($W/m^2 K$) |
| h_m | = mass transfer constant ($W/m^2 K$) |

Subscripts

| | | | |
|---|-------------|---|----------------|
| r | = relative | p | = particle |
| a | = air | v | = water vapor |
| c | = capillary | l | = liquid water |
| g | = gas | | |

References

- [1] Kaviany, M. Principle of Heat Transfer in Porous Media. Springer, New York, 1991.
- [2] Nield, D.A. and Bejan, A.. Convective in Porous Media. Springer-Verlag, New York, 1991.
- [3] Whitaker, S. A Theory of Drying in Porous Media. Adv. Heat Transfer, 13, 1977, pp.119-203.
- [4] Patankar, S.V., 1980 . Numerical Heat Transfer and Fluid Flow. McGraw-Hill. New York, Chaps.1-4.
- [5] Boukadida, N., S. Ben Nasrallah and P. Perre., 2000. Mechanism of Heat and Mass Transfer During Convective Drying of Porous Media under Different Drying Conditions. Drying Technology . Vol. 18, pp. 1367-1388.
- [6] Perr, P., and I.W. Turner, A3D version of TransPore, A Comprehensive Heat and Mass Transfer Computational Model For Simulating the Drying of Porous Media., Int. J. Heat and Mass Transfer, 24, 4501, 1999.
- [7] Ratanadecho, .P, Aoki, K.and Akahori, M., 2002. The Characteristics of Microwave Melting of Frozen Packed Beds Using a Rectangular Waveguide. IEEE Transactions on microwave theory and techniques. Vol.50, No.6, pp.1495-1502.
- [8] Ratanadecho, P., Aoki, K. and Akahori, M..Experimental and Numerical Study of Microwave Drying in Unsaturated Porous Material. Int, Commun. Heat and Mass Transfer, Vol.28 (5), 2001, pp.605-616.
- [9] Ratanadecho, .P, Aoki, K.and Akahori, M., 2002. Influence of Irradiation Time, Particle Sizes, and Initial Moisture Content During Microwave Drying of Multi-Layered Capillary Porous Materials. Journal of Heat Transfer. Vol. 124, pp.151-161.
- [10] P.Perre, M.Moser and M.Martin, Advances in transport phenomena during convective drying with superheated steam, Int. J. Heat Mass Transfer. Vol.36, No.11, pp2725-2746, 1993.
- [11] S.Ben Nasrallah and P. Perre, Detailed study of a model of heat and mass transfer during convective drying of porous media, Int .J. Heat Mass Transfer., Vol.31, No.5, pp957-967, 1988.
- [12] C.L.D. Huang, Gamal N. Ahmed and D.L.Fenton, Responses of concrete walls to fire, Int. J. Heat Mass Transfer., Vol.34, No.3, pp649-661, 1991.